Journal of Colloid and Interface Science 418 (2014) 366–372

Contents lists available at ScienceDirect

Journal of Colloid and Interface Science

www.elsevier.com/locate/jcis

Poly (vinylsulfonic acid) assisted synthesis of aqueous solution stable vaterite calcium carbonate nanoparticles

Ashvin T. Nagaraja [a], Sulolit Pradhan [a], Michael J. McShane [a,b,*]

[a] Department of Biomedical Engineering, Texas A&M University, College Station, TX 77843, United States
[b] Materials Science and Engineering Program, Texas A&M University, College Station, TX 77843, United States

ARTICLE INFO

Article history:
Received 23 July 2013
Accepted 3 December 2013
Available online 21 December 2013

Keywords:
Poly (vinylsulfonic acid)
Vaterite
Calcium carbonate
Nanoparticle
Nucleation
Co-precipitation

ABSTRACT

Calcium carbonate nanoparticles of the vaterite polymorph were synthesized by combining $CaCl_2$ and Na_2CO_3 in the presence of poly (vinylsulfonic acid) (PVSA). By studying the important experimental parameters we found that controlling PVSA concentration, reaction temperature, and order of reagent addition the particle size, monodispersity, and surface charge can be controlled. By increasing PVSA concentration or by decreasing temperature CCNPs with an average size from ≈150 to 500 nm could be produced. We believe the incorporation of PVSA into the reaction plays a dual role to (1) slow down the nucleation rate by sequestering calcium and to (2) stabilize the resulting CCNPs as the vaterite polymorph, preventing surface calcification or aggregation into microparticles. The obtained vaterite nanoparticles were found to maintain their crystal structure and surface charge after storage in aqueous buffer for at least 5 months. The aqueous stable vaterite nanoparticles could be a useful platform for the encapsulation of a large variety of biomolecules for drug delivery or as a sacrificial template toward capsule formation for biosensor applications.

1. Introduction

Calcium carbonate is an important material for fundamental and applied study, with implications in industrial [1], household [2], and biological processes [3]. Calcium carbonate exists as three different anhydrous polymorphs: calcite, aragonite and vaterite in order of increasing solubility and decreasing thermodynamic stability. Nanoporous calcium carbonate particles have attracted much attention because of their biocompatibility, high effective surface area, ability to protect encapsulated components, larger pore size than mesoporous silica, inexpensive production under ambient conditions, and ease of dissolution with mild treatment of EDTA at neutral pH [4]. There is significant interest in producing the vaterite polymorph of calcium carbonate because it has better water solubility, higher porosity, and is more easily dissolved than calcite or aragonite. However, the thermodynamic instability of vaterite makes its natural occurrence rare, requiring kinetic stabilization even for laboratory production. Investigation into different crystal growth modifiers for vaterite formation is encompassed by the vast literature studying additive-directed crystallization [5,6], for its importance in understanding mesocrystal formation for biomineralization [7,8]. It is difficult to predict the outcome of different additives from theory; hence, most understanding is gained through empirical observations. Additional factors such as concentration and ratio of Ca^{2+} to CO_3^{2-}, temperature, pH, reaction duration, and mixing speed all influence the outcome and further complicate understanding the process. Polymers act to inhibit or stabilize specific crystal structures, reshaping and directing crystal formation depending on chemical composition, charge density, and concentration [9]. A wide variety of structures and crystal polymorphs can be produced, with even a small amount of additive having a significant influence on the outcome. Copolymers containing both interacting and stabilizing components reshape crystallization based on the affinity of the chemical structure for the mineral salt ions and crystal faces [10]. In recent work, the commercial random copolymer poly (4-styrenesulfonate-co-maleic acid) (PSS-co-MA) was found to direct crystallization to produce a variety of superstructures depending on its relative concentration to calcium in the reaction [8,11]. A PEI assisted ultrasonic method was developed for the synthesis of vaterite microparticles that were stable for at least 8 months [12]. Other commonly used polyelectrolytes used include carboxylic or sulfate containing synthetic and biopolymers [13,14].

Abbreviations: PVSA, poly (vinylsulfonic acid); CCNP, calcium carbonate nanoparticle; DLS, dynamic light scattering; NTA, nanoparticle tracking analysis; BET, Brunauer–Emmett–Teller.

* Corresponding author. Address: 5045 Emerging Technologies Building, 3120 TAMU, College Station, TX 77843, USA. Fax: +1 979 845 4450.

E-mail addresses: ashvin.nagaraja@gmail.com (A.T. Nagaraja), sulolitp@gmail.com (S. Pradhan), mcshane@tamu.edu (M.J. McShane).

0021-9797/$ - see front matter © 2013 Elsevier Inc. All rights reserved.
http://dx.doi.org/10.1016/j.jcis.2013.12.008

For biosensor or drug delivery applications the production of spherical vaterite is desired because the highly porous structure can serve as a template for biomolecule incorporation. Encapsulation into these particles is achieved either by adsorption to the highly porous structure after particle formation [15] or by addition during nucleation to coprecipitate during particle formation [16]. In many cases, the biomolecule-encapsulating calcium carbonate microparticle is used as a template to create hollow capsules by the sequential deposition of oppositely charged polyelectrolytes using electrostatic layer-by-layer, followed by core dissolution [17]. Applications of calcium carbonate nanoparticles (CCNPs) would have vast implications for both drug delivery and sensor applications. In order for a drug-carrying nanoparticle to passively enter a subcutaneous tumor cell it must be less than the 200–1200 nm pore size cutoff [18]. For competitive binding glucose biosensors, compartmentalization of macromolecules into nanocapsules should improve response times by decreasing diffusion distances [19].

Production of CCNPs requires decreasing the particle growth rate and stabilizing the NPs before they agglomerate to form microparticles or recrystallize to calcite. Alginate chains have been used to reduce the nucleation growth rate by sequestering calcium, resulting in the formation of CCNPs [20]. However, the resulting CCNPs showed an increase in size and loss of negative surface charge after 4 h in aqueous solution, indicating surface recrystallization. Ethylene glycol was used to reduce the solubility and crystal growth rate of calcium carbonate to produce vaterite nanoparticles down to 430 nm in size [21]. These particles remained as vaterite in ethanol, but recrystallized to calcite when transferred to aqueous solutions. Thus, while a few examples of efforts to produce CCNPs have been reported, we have not identified any that yield long-term aqueous stable vaterite nanoparticles.

The focus of this work was to study the effect of poly (vinylsulfonic acid) (PVSA) on CCNP formation and production of vaterite nanoparticles. It has been shown that the presence of sulfonic groups on polymers stabilizes the vaterite structure [2]. We hypothesized that incorporation of commercially available PVSA, a low-molecular-weight and high-charge-density polyelectrolyte, would limit interparticle bridging and aggregation of primary nuclei to prevent microparticle formation. This idea was based on a previous report of the copolymer of PVSA and chitosan which found that the sulfonate groups strongly interacted with and attached to the calcium carbonate surface [22]. Here we describe a method to obtain vaterite CCNPs and report how PVSA concentration, reaction temperature, and order of reagent addition affect particle size, morphology, surface charge, and crystalline structure.

2. Experimental section

2.1. Chemicals

PVSA (Sigma) was filtered through a 0.2 μM syringe filter prior to use. Na_2CO_3 and $CaCl_2$ (Sigma) was used as received. PVSA molecular weight of 4000–6000 kDa according to manufacturer's specifications, 5000 kDa was used for calculations.

2.2. CCNP synthesis

About 10 ml of 20 mM Na_2CO_3 and PVSA were added to a 100 ml beaker and stirred at 800 RPM with a spinning wedge stir bar (VWR). After 1 min, 10 ml of 20 mM $CaCl_2$ was rapidly injected. The beaker was covered and the solution was allowed to react at RT for 1–14 h depending on the PVSA concentration (Table S1). The mixture was transferred to 50 ml conical tube and centrifuged at 10,000 g for 5 min to recover the formed particles and remove unreacted components. The particles were washed 3 times with 50 mM pH 9 Tris buffer and finally resuspended as a 1 ml stock solution in 50 mM pH 9 Tris buffer. This process was also done in reverse where $CaCl_2$ was added first followed by PVSA and then Na_2CO_3 (Table S2).

2.3. Scanning electron microscopy (SEM)

Images were obtained with a JEOL FE-SEM 7500. 2 μl of a 1/10 diluted stock dilution was placed on a cleaned silica support and dried in a vacuum chamber overnight followed by gold sputtering for 45 s.

2.4. XRD

The X-ray source was a 2.2 kW Cu X-ray tube, maintained at an operating current of 40 kV and 40 mA. The standard Bragg–Brentano para-focusing mode with the X-ray diverging from a DS slit (1 mm) at the tube to strike the sample and then converging at a position sensitive X-ray Detector (Lynx-Eye, Bruker-AXS). The two-circle 250 mm diameter goniometer was computer controlled with independent stepper motors and optical encoders for the θ and 2θ circles with the smallest angular step size of $0.0001°2\theta$. Data collection was automated COMMANDER program by employing a DQL file and was analyzed by the program EVA.

2.5. DLS and ζ-potential

Dynamic Light Scattering (DLS) and ζ-potential was measured using a Zeta Sizer Nano Series ZEN 3600 Spectrometer (Malvern Instruments Ltd., Malvern, Worcestershire, United Kingdom). A 1 ml, 1/20 diluted stock solution in 5 mM pH 9.0 Tris buffer was used for measurement.

2.6. Nanoparticle tracking analysis (NTA)

Particle size and distributions were obtained with the NanoSight LM10HS with a 65 mW 405 nm source. A 300 μl sample of a 1/100 dilution of the sample stock solution in 0.1 M bicarbonate buffer was used for analysis. Video was acquired with a Hamamatsu C11440 digital camera for 3 min in order to obtain at least 1000 particle tracking events. Analysis was completed with included NanoSight 2.3 software with automatic settings.

2.7. UV–VIS spectroscopy

UV–VIS absorbance was obtained on a Cary 300 UV–VIS spectrophotometer with a 6×6 multi-cell peltier block and temperature controller. For the time dependent studies a scaled down reaction in a 3 ml total volume (1.5 ml $CaCl_2$, 1.5 ml Na_2CO_3, and PVSA) was monitored at 500 nm at 20–30 s intervals under constant stirring.

2.8. Brunauer–Emmett–Teller (BET) method

The surface area and pore size of the $CaCO_3$ nanoparticles was determined using the BET method with nitrogen adsorption and desorption at 77 K using a Micromeritics ASAP 2000.

3. Results

The simple experimental setup is depicted in Scheme 1 where equal volumes of equimolar of $CaCl_2$ and Na_2CO_3 are combined under agitation in the presence of PVSA. In the first set of experiments 10 mLs of 0.02 M Na_2CO_3 was combined with PVSA in a beaker and

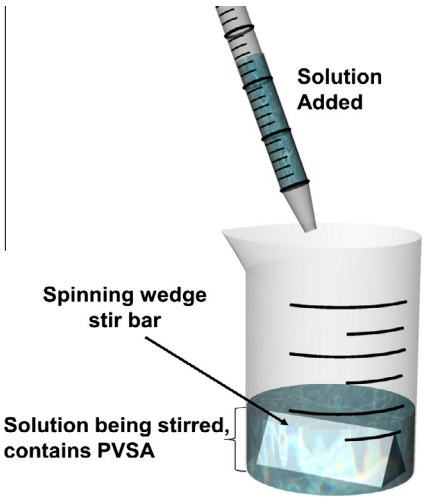

Scheme 1. Schematic of experimental setup where PVSA, Na_2CO_3 and $CaCl_2$ are combined in a beaker under agitation with a spinning wedge stir bar.

stirred at 800 RPM (stirred solution) for 2 min. Then 10 mLs of 0.02 M $CaCl_2$ was rapidly injected (solution added) and the reaction was incubated under constant stirring at room temperature.

The concentration of PVSA in the stirred solution was varied in order to understand how particle size and morphology would be affected. The mixing of $CaCl_2$ and Na_2CO_3 without any additive results in immediate particle formation apparent from the increased turbidity, but the incorporation of PVSA into the reaction significantly delays the onset of the nucleation.

To understand the process, a scaled-down reaction was performed in a cuvette and monitored with UV–VIS absorbance spectroscopy. The results reported in Fig. 1 shows the time dependent absorption at 500 nm, which is a measure of turbidity and, hence, particle formation or growth. At PVSA concentrations from 0.16 to 1.24 μM there is no apparent particle formation for ≈5–6 min (indicated by the sharp increase in absorbance) and at 1.84 μM it takes ≈150 min for notable particle formation. With increasing PVSA concentrations from 0.16 to 1.84 μM we also observe a decrease in the peak steady-state absorbance reached that indicates the production of either smaller sized or fewer particles. At 2.43 μM and 3.01 μM PVSA the growth pattern changes: instead of a delay followed by a sharp inflection, a continuous slow growth was observed. A higher reaction slope was observed for the higher PVSA concentration, a trend which continues to at least 4.14 μM. The minimum incubation time required for each PVSA

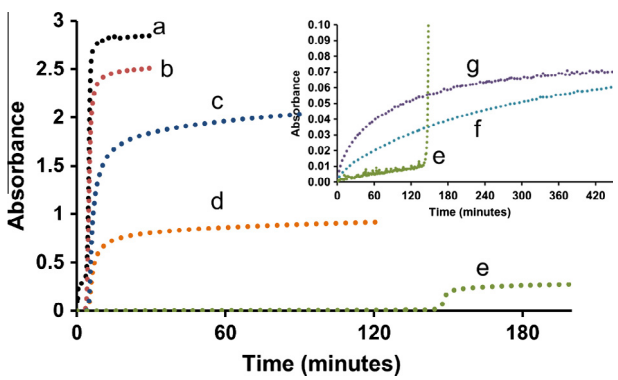

Fig. 1. Time dependent absorbance at 500 nm for the reaction maintained at 25 °C under constant stirring for different PVSA concentrations (a) 0.16 μM (b) 0.31 μM, (c) 0.62 μM, (d) 1.24 μM, (e) 1.84 μM, (f) 2.43 μM, and (g) 3.01 μM.

concentration before recovery of the particles by centrifugation was determined by finding the time when the absorbance increase reached steady-state (first derivative equal to 0) (Table S1). After centrifugation at 10,000 g for 5 min, the particles were washed 3 times and suspended in a concentrated 1 ml stock solution for further analysis. The particles were stored in an alkaline buffered solution to prevent acidic dissolution of particles. Particle morphology was determined by SEM imaging of CCNPs suspended on a silica wafer and gold sputter coated. For the lower PVSA concentrations (Fig. 2a–d) the particles exhibit spherical morphology associated with vaterite. The surface appears porous and looks very similar to other reports of calcium carbonate microparticles. At higher PVSA concentrations (Fig. 2e and f) particles cannot be distinctly observed; therefore, size and morphology are not distinguishable because the small particles aggregate during sample drying. For all PVSA concentrations, no calcite rhombohedra were found in the populations observed.

Dynamic light scattering (DLS) was used as a rapid method to determine the size of the CCNPs for different PVSA concentrations. The results reported in Fig. 3A shows the change in average size by intensity and size peak by number of the resulting particles formed. As concentration of PVSA was increased from 0.16 to 1.84 μM, peak size by number shows a slight downward trend but no significant differences were observed. Particles were all above 300 nm average diameter. At a concentration between 1.84 and 2.43 μM, an apparent threshold is crossed and peak size by number decreases to less than 150 nm. No significant change in size was found with further increase in PVSA concentration. Characterization of CCNPs with nanoparticle tracking analysis (NTA) was obtained (Fig. 3B) to gain further understanding of hydrodynamic particle size. A limitation of DLS is the intensity based measurement which is weighted towards the higher scattering cross section of larger particles [23]. By tracking individual particle movement NTA provides additional understanding of particle size and size distribution. From these data we observe that increasing PVSA concentration decreases peak particle size but there are some larger particles present even at higher PVSA concentrations.

To understand how order of addition affects the reaction dynamics the experiments were repeated for each PVSA concentration using the same setup in Scheme 1 but instead with $CaCl_2$ and PVSA as the stirred solution and Na_2CO_3 as the solution added. The SEM images (Fig. 4a–d) of the resulting CCNPs reveal the spherical morphology, but again at higher PVSA concentrations (Fig. 4e and f) a clear distinction between particles was not observed.

The DLS results for particles produced when $CaCl_2$ was the stirred solution (Fig. 5A) show a similar trend and threshold transition to what was observed previously when Na_2CO_3 was the stirred solution. However, as PVSA concentration increases we observe smaller particle size by number and intensity and less error between triplicates compared to when Na_2CO_3 was the stirred solution. There is also less divergence between intensity and number distribution measurements, indicating less aggregation and greater monodispersity. From NTA (Fig. 5B) we observe that at lower PVSA concentrations (0.15 μM and 0.62 μM) a broad multimodal distribution is present, but at higher PVSA concentrations (2.43 μM and 4.13 μM) average particle size decreases and becomes more monodisperse.

XRD data were obtained for particles produced with 0.62 μM PVSA when Na_2CO_3 (Fig. 6a) or $CaCl_2$ (Fig. 6b) was the stirred solution. All peaks on the diffraction spectra were associated with vaterite, indicating that the nanoparticles produced are of the desired vaterite polymorph. It is also noteworthy that the data shown were obtained from samples after storage for 5 months in pH 9 Tris buffer at room temperature. This indicates that the PVSA has stabilized the particles to prevent calcification for an extended period of time.

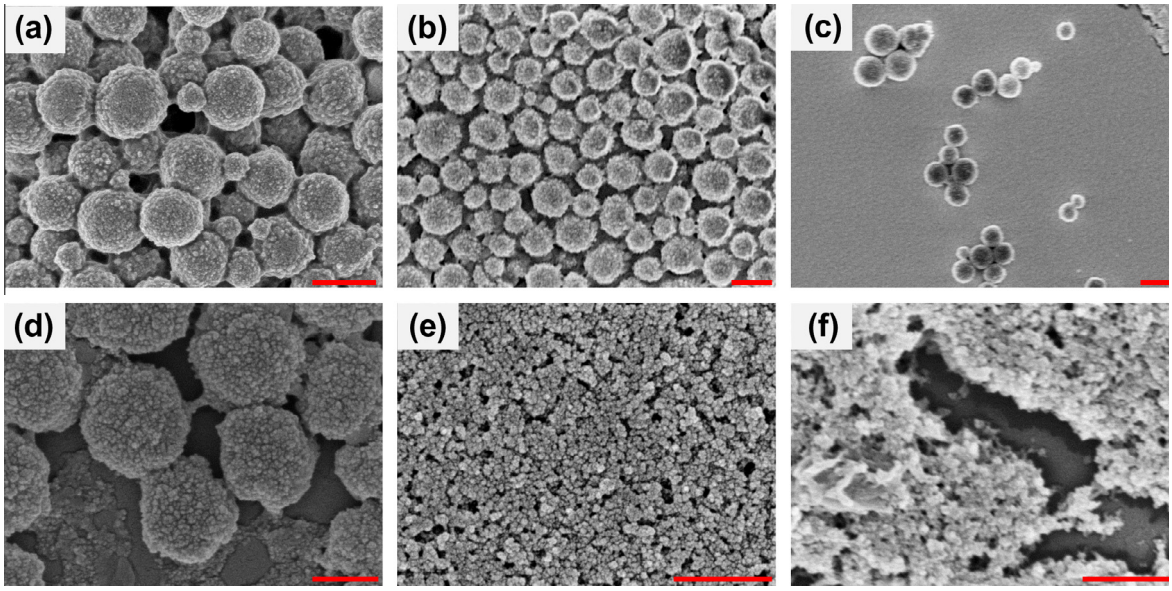

Fig. 2. SEM images of sputter coated CCNPs produced when Na_2CO_3 was the stirred solution for different PVSA concentrations (a) 0.31 μM, (b) 0.62 μM, (c) 1.24 μM, (d) 1.84 μM, (e) 2.43 μM, and (f) 3.01 μM. Scale bars correspond to 500 nm.

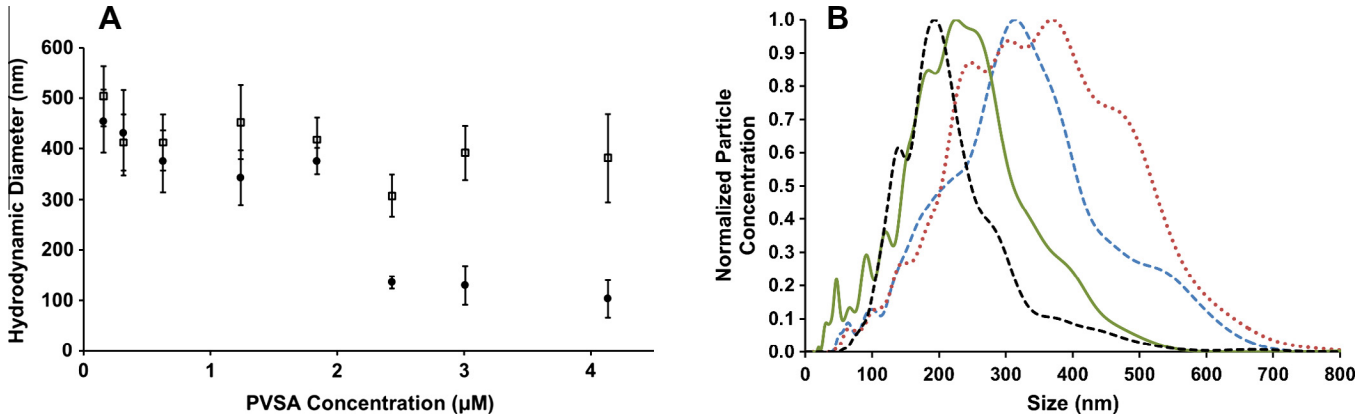

Fig. 3. (A) DLS results represent average size by intensity (□) and size peak by number (●) for CCNPs at different PVSA concentrations when Na_2CO_3 was the stirred solution. Error bars represent 95% confidence intervals for three separate batches of particles. (B) NTA plots showing changes in size distribution at 0.15 μM (blue - -), 0.62 μM (red ●), 2.43 μM (green –), and 4.13 μM (black - -) PVSA when $CaCl_2$ was the stirred solution. (For interpretation of the references to color in this figure legend, the reader is referred to the web version of this article.)

BET analysis of CCNPs produced with 0.62 μM PVSA and $CaCl_2$ as the stirred solution revealed a surface area of 33.88 m^2/g, a single point pore volume of 0.065 cm^3/g, and an average pore size of 10.4 nm (Fig. S1). Interestingly, PVSA-stabilized CCNPs have a surface area higher than reported values for calcium carbonate microparticles (6.18 and 8.8 m^2/g) [24,25] and other vaterite CCNPs (400 nm diameter, 22 m^2/g) [26], but have a smaller average pore size than both (13.78 nm and 35 nm for microparticles, 35 nm for CCNPs). The high surface area and porous nature of these CCNPs make them a suitable reservoir for material encapsulation.

Zeta potential measurements for particles made in both $CaCl_2$ and Na_2CO_3 as the stirred solutions are reported in Fig. 7. When Na_2CO_3 was the stirred solution we observe an increasing magnitude of a negative zeta potential with increasing PVSA concentration, indicating more surface coverage by PVSA. In contrast, when $CaCl_2$ is the stirred solution the zeta potential remains at ≈20 mV until the highest PVSA concentration. The sequestration of calcium by PVSA is either preventing complete adsorption of polymer on the CCNP surface or is neutralizing some of the surface charge. The particles had a negative surface charge for all PVSA concentrations and maintained this charge even after 5 months of storage in Tris buffer (time of this measurement), indicating the PVSA has stabilized the surface to prevent calcification.

The influence of temperature on the reaction rate kinetics and resulting particle size and size distribution were studied using both UV–VIS spectroscopy and NTA. The time dependent nucleation when Na_2CO_3 was the stirred solution (Fig. 8A) at three different temperatures shows that by decreasing temperature from 25 °C to 5 °C the onset of nucleation is delayed and the peak steady-state absorbance reached is less. The first derivative of the time dependent reaction (inset of Fig. 8A) shows that the peak reaction rate reached is also decreasing with decreasing temperature. Sizing with NTA (Fig. 8B) revealed that decreasing temperature decreased the CCNPs peak size to less than 200 nm at 5 °C (Table S3). Decreasing temperature also greatly improves the monodispersity decreasing the coefficient of variance from 107.7% at 25 °C to 24.5% at 5 °C. When $CaCl_2$ was the stirred solution (Fig. 8C) there was a longer delay in the onset of peak nucleation compared to

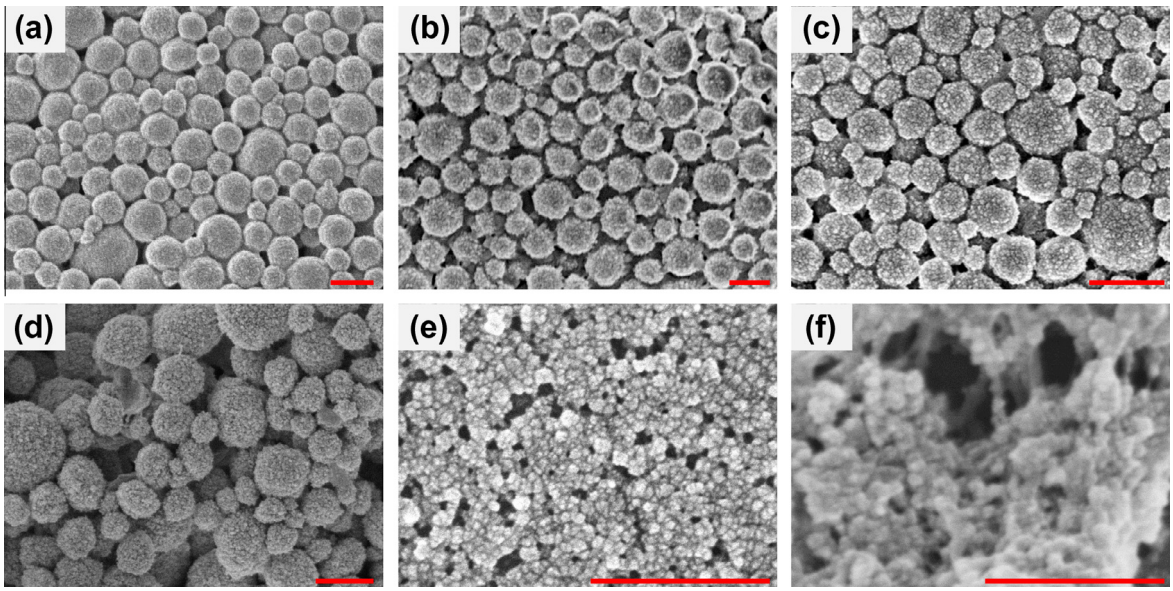

Fig. 4. SEM images of sputter coated CCNPs produced when $CaCl_2$ was the stirred solution for different PVSA concentrations (a) 0.31 μM, (b) 0.62 μM, (c) 1.24 μM, (d) 1.84 μM, (e) 2.43 μM, and (f) 3.01 μM. Scale bars correspond to 500 nm.

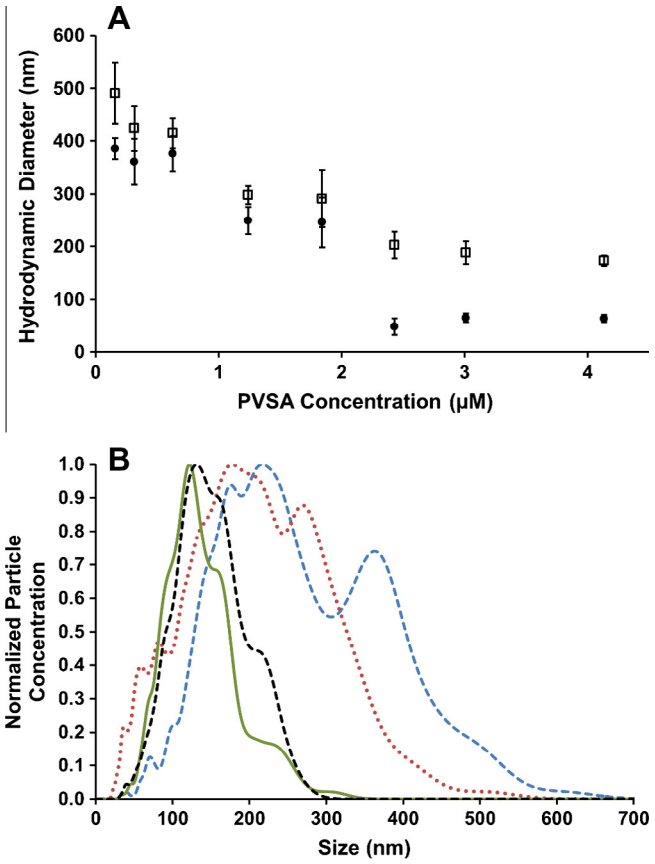

Fig. 5. (A) DLS results represent average size by intensity (□) and size peak by number (●) for CCNPs at different PVSA concentrations when $CaCl_2$ was the stirred solution. Error bars represent 95% confidence intervals for three separate batches of particles. (B) NTA plots showing changes in size distribution at 0.15 μM (blue - -), 0.62 μM (red ●), 2.43 μM (green –), and 4.13 μM (black - -) PVSA when $CaCl_2$ was the stirred solution. (For interpretation of the references to color in this figure legend, the reader is referred to the web version of this article.)

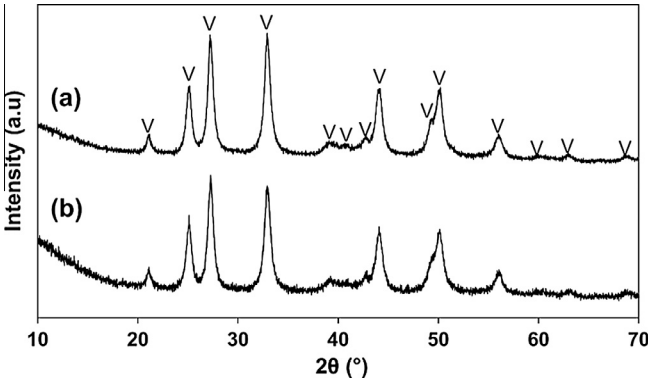

Fig. 6. XRD of CCNPs formed when (a) Na_2CO_3 or (b) $CaCl_2$ was the stirred solution for 0.62 μM PVSA. Peaks associated with the vaterite polymorph are marked with a (V).

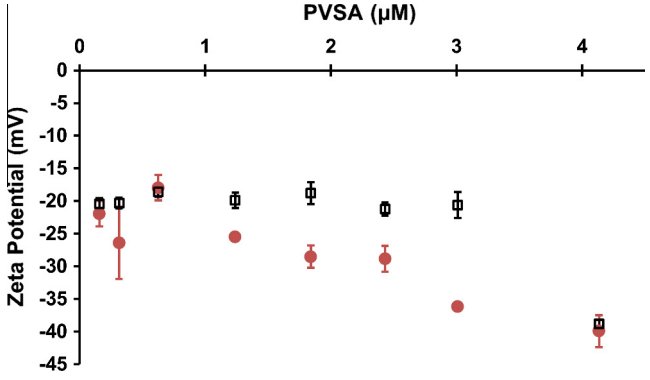

Fig. 7. Zeta potential measurements for $CaCl_2$ (black □) or Na_2CO_3 (red ●) as the stirred solution. Error bars represent 95% confidence intervals for three separate batches of particles. (For interpretation of the references to color in this figure legend, the reader is referred to the web version of this article.)

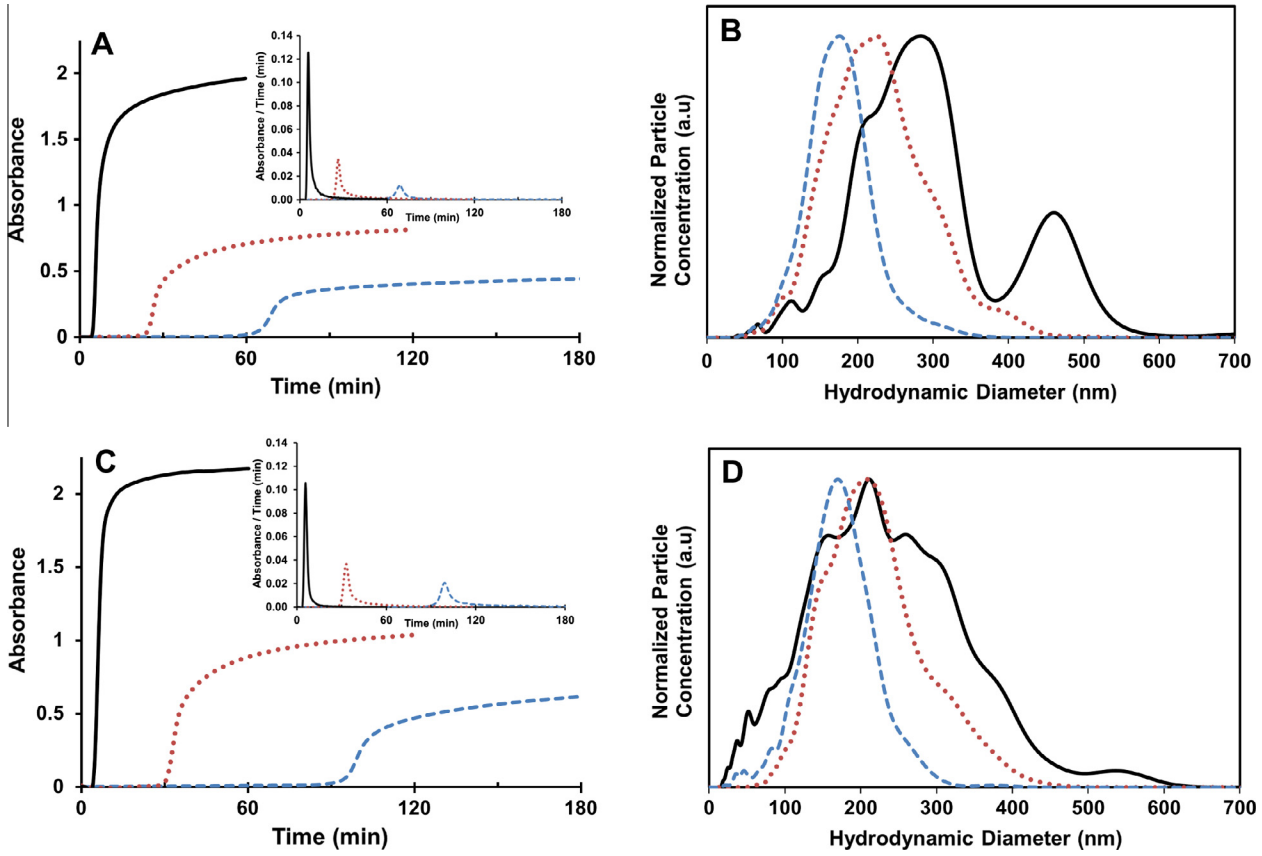

Fig. 8. Time dependent UV–VIS absorbance at 500 nM monitoring the nucleation and (inset) first derivative when (A) Na_2CO_3 or (C) $CaCl_2$was the stirred solution and NTA plots of CCNPs produced for 0.62 μM PVSA when (B) Na_2CO_3 or (D) $CaCl_2$ was the stirred solution at 5 °C (blue –), 10 °C (red ●), and 25 °C (black -). (For interpretation of the references to color in this figure legend, the reader is referred to the web version of this article.)

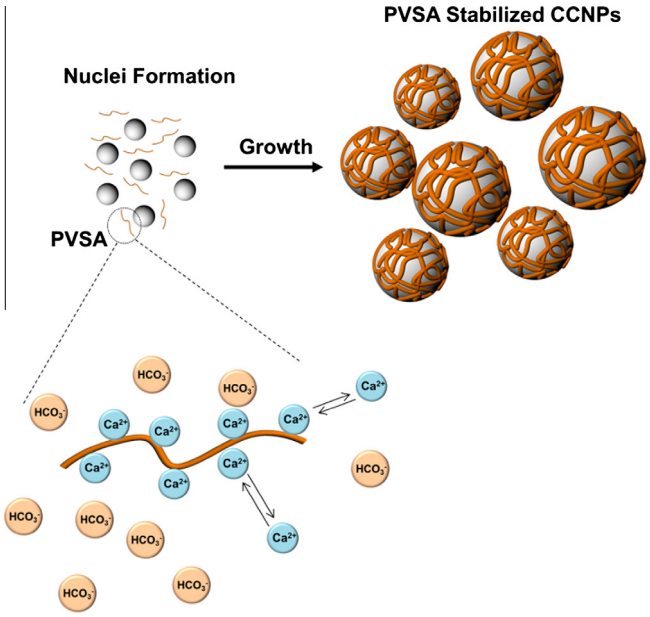

Scheme 2. Proposed mechanism of PVSA assisted growth wherein PVSA plays a dual role to: (1) sequester calcium through ionic interactions to slow down nucleation rate and (2) stabilize the resulting nanoparticles to prevent agglomeration into microparticles or recrystallize into calcite.

Na_2CO_3, but a similar trend with decreasing temperature. NTA again reveals the smaller peak size and decrease in the coefficient of variance with decreasing temperature from 42.5% at 25 °C to 27% at 4 °C (Fig. 8D).

4. Conclusions

We have demonstrated an easy and rapid method to synthesize CCNPs requiring no specialized chemicals, equipment, or setup. We have shown that size of particles produced can by selected by controlling PVSA concentration. The PVSA is stabilizing the particles in solution as the vaterite polymorph with a strong negative surface charge and maintains this crystal structure and surface charge even when stored in a buffered solution for up to 5 months. This is an important distinction primarily because other methods that produced vaterite CCNPs were not stable in water [20,21]. Gas adsorption measurements revealed that while PVSA-stabilized CCNPs have a high surface area compared to other calcium carbonate particles, the average pore size is smaller than expected (less than 10 nm). The time dependent analysis revealed the kinetics of particle formation and growth, including the influence of different concentrations of PVSA as well as different temperatures. Increasing the PVSA concentration or decreasing the temperature both delayed the onset of the peak nucleation rate as well as decreased the reaction rate. Decreasing reaction temperature provides an easy method to further decrease size and greatly improve monodispersity. The difference in result when either

$CaCl_2$ or Na_2CO_3 was the stirred solution is interesting because when no additive is present it should not matter. However, when an additive is involved it is important to consider its interaction with the two components. The interaction of PVSA with calcium causes dependence on order of addition that affects the outcome of particle size, monodispersity, and surface charge. While better control on size is achieved when $CaCl_2$ is the stirred solution, a more negative surface charge was attained when Na_2CO_3 was the stirred solution. Interestingly, at 5 °C the difference in particle size and distribution when Na_2CO_3 or $CaCl_2$ was the stirred solution was much less than at 25 °C. Hence, the difference in order of addition can be mitigated by decreasing reaction temperature.

From the results reported in this paper we suspect that PVSA is playing a dual role in (1) slowing the nucleation growth rate by sequestering excess calcium and (2) stabilizing the resulting CCNPs to prevent surface calcification and aggregation to form microparticles (Scheme 2). As free calcium complexes with carbonate to form particles the concentration gradient causes more sequestered calcium to be released. This results in a feeding process, which acts to control growth. Eventually the PVSA is no longer charge shielded by the free calcium and it then binds to the particle surface. The polymer imparts a high surface charge density and electrostatic repulsion between nanoparticles to prevent aggregation into microparticles.

Future work will focus on encapsulation of nanomaterials and biomolecules both with adsorption and co-precipitation for use as a template for capsule formation. We expect a tradeoff between particle size and encapsulation efficiency that will require further optimization of experimental conditions and possibly the development of a multiphase process where temperature and PVSA concentration are dynamically controlled.

5. Author contributions

The manuscript was written through contributions of all authors. All authors have given approval to the final version of the manuscript.

Acknowledgments

This material is based upon work supported by the National Science Foundation under Grant No. (1066928). Use of the TAMU Materials Characterization Facility is acknowledged. The X-ray diffractometers, small angle scattering instrumentation and crystallographic computing systems in the X-ray Diffraction Laboratory at the Department of Chemistry, Texas A&M University were purchased with funds provided by the National Science Foundation (CHE-9807975, CHE-0079822 and CHE-0215838). We gratefully acknowledge Prof. Hae-Kwon Jeong and Hyuk-Taek Kwon for guidance and technical assistance with the BET surface area and pore size analysis.

Appendix A. Supplementary material

Supplementary data associated with this article can be found, in the online version, at http://dx.doi.org/10.1016/j.jcis.2013.12.008.

References

[1] A. Martinod, M. Euvrard, A. Foissy, A. Neville, Desalination 220 (2008) 345–352.
[2] D. Verdoes, R.C. Van Landschoot, G.M. Van Rosmalen, J. Cryst. Growth 99 (1990) 1124–1129.
[3] J.W. Morse, R.S. Arvidson, A. Luttge, Chem. Rev. 107 (2007) 342–381.
[4] Y. Wang, A.D. Price, F. Caruso, J. Mater. Chem. 19 (2009) 6451–6464.
[5] K. Naka, Y. Chujo, Chem. Mater. 13 (2001) 3245–3259.
[6] R.-Q. Song, H. Cölfen, CrystEngComm 13 (2011) 1249–1276.
[7] M. Niederberger, H. Colfen, Phys. Chem. Chem. Phys. 8 (2006) 3271–3287.
[8] R.Q. Song, H. Colfen, Adv. Mater. 22 (2010) 1301–1330.
[9] R.Q. Song, H. Colfen, A.W. Xu, J. Hartmann, M. Antonietti, ACS Nano 3 (2009) 1966–1978.
[10] E. Dalas, P. Klepetsanis, P.G. Koutsoukos, Langmuir 15 (1999) 8322–8327.
[11] R.Q. Song, A.W. Xu, M. Antonietti, H. Colfen, Angew. Chem. 48 (2009) 395–399.
[12] A. López-Marzo, J. Pons, A. Merkoçi, J. Mater. Chem. 22 (2012) 15326–15335.
[13] J.L. Arias, A. Neira-Carrillo, J.I. Arias, C. Escobar, M. Bodero, M. David, M.S. Fernandez, J. Mater. Chem. 14 (2004) 2154–2160.
[14] M.F. Butler, N. Glaser, A.C. Weaver, M. Kirkland, M. Heppenstall-Butler, Cryst. Growth Des. 6 (2006) 781–794.
[15] D.V. Volodkin, N.I. Larionova, G.B. Sukhorukov, Biomacromolecules 5 (2004) 1962–1972.
[16] A.I. Petrov, D.V. Volodkin, G.B. Sukhorukov, Biotechnol. Prog. 21 (2005) 918–925.
[17] G.B. Sukhorukov, D.V. Volodkin, A.M. Gunther, A.I. Petrov, D.B. Shenoy, H. Mohwald, J. Mater. Chem. 14 (2004) 2073–2081.
[18] S.K. Hobbs, W.L. Monsky, F. Yuan, W.G. Roberts, L. Griffith, V.P. Torchilin, R.K. Jain, Proc. Natl. Acad. Sci. 95 (1998) 4607–4612.
[19] R.J. Russell, M.V. Pishko, C.C. Gefrides, M.J. McShane, G.L. Coté, Anal. Chem. 71 (1999) 3126–3132.
[20] D. Zhao, R.X. Zhuo, S.X. Cheng, Mol. BioSyst. 8 (2012) 753–759.
[21] B.V. Parakhonskiy, A. Haase, R. Antolini, Angew. Chem. Int. Ed. 51 (2012) 1195–1197.
[22] A. Neira-Carrillo, P. Mercade-Jaque, M. Diaz-Dosque, C. Tapia-Villanueva, M. Yazdani-Pedram, J. Iran. Chem. Soc. 8 (2011) 811–824.
[23] J.A. Gallego-Urrea, J. Tuoriniemi, M. Hassellöv, TrAC, Trends Anal. Chem. 30 (2011) 473–483.
[24] D.V. Volodkin, A.I. Petrov, M. Prevot, G.B. Sukhorukov, Langmuir 20 (2004) 3398–3406.
[25] S. Kim, J.W. Ko, C.B. Park, J. Mater. Chem. 21 (2011) 11070.
[26] B.V. Parakhonskiy, C. Foss, E. Carletti, M. Fedel, A. Haase, A. Motta, C. Migliaresi, R. Antolini, Biomater. Sci. (2013).